

Random focusing of nonlinear acoustic N -waves in fully developed turbulence: Laboratory scale experiment

Mikhail Averiyarov^{a)}

Faculty of Physics, Moscow State University, 119991 Moscow, Russia

Sébastien Ollivier

LMFA UMR CNRS 5509, Ecole Centrale de Lyon, Université de Lyon, 36 Avenue Guy de Collongue, F-69134 Ecully Cedex, France

Vera Khokhlova^{b)}

Faculty of Physics, Moscow State University, 119991 Moscow, Russia

Philippe Blanc-Benon

LMFA UMR CNRS 5509, Ecole Centrale de Lyon, Université de Lyon, 36 Avenue Guy de Collongue, F-69134 Ecully Cedex, France

(Received 3 March 2011; revised 29 August 2011; accepted 19 September 2011)

A laboratory experiment was conducted to study the propagation of short duration ($25 \mu\text{s}$) and high amplitude (1000 Pa) acoustic N -waves in turbulent flow. Turbulent flows with a root-mean-square value of the fluctuating velocity up to 4 m/s were generated using a bidimensional nozzle ($140 \times 1600 \text{ mm}^2$). Energy spectra of velocity fluctuations were measured and found in good agreement with the modified von Kármán spectrum for fully developed turbulence. Spherical N -waves were generated by an electric spark source. Distorted waves were measured by four 3 mm diameter microphones placed beyond the turbulent jet. The presence of turbulence resulted in random focusing of the pulse; more than a threefold increase of peak pressures was occasionally observed. Statistics of the acoustic field parameters were evaluated as functions of the propagation distance and the level of turbulence fluctuations. It is shown that random inhomogeneities decrease the mean peak positive pressure up to 30% at 2 m from the source, double the mean rise time, and cause the arrival time about 0.3% earlier than that for corresponding conditions in still air. Probability distributions of the pressure amplitude possess autosimilarity properties with respect to the level of turbulence fluctuations. © 2011 Acoustical Society of America. [DOI: 10.1121/1.3652869]

PACS number(s): 43.28.Gq, 43.25.Jh, 43.28.Mw [VEO]

Pages: 3595–3607

I. INTRODUCTION

Propagation of high amplitude acoustic waves through atmospheric turbulence is an important problem for fundamental nonlinear wave physics. In outdoor sound propagation, the importance of wind in acoustics has been known since the end of the 19th century, when initial studies on effective sound speed and formation of shadow zones were performed based on observations of various sources of intense sound like volcanic eruptions, thunder, explosions, and artillery fire.¹ While propagating in turbulent air, acoustic waves are distorted by the combined effects of diffraction and scattering by atmospheric inhomogeneities,^{2–5} nonlinear dissipation,^{6,7} and linear absorption/relaxation.^{8,9} At sufficiently long propagation distances multiple focusing of acoustic waves is predicted.^{10–12} Nonlinear and diffraction effects become even more important at foci (caustics),^{13–15} where the acoustic pressure level increases. To predict shock

wave pressures in inhomogeneous media, it is thus important to understand the relative influence of different physical mechanisms involved in wave propagation.^{16–19} Accurately controlled experiments are needed for this purpose and also to validate theoretical models for nonlinear sound propagation in inhomogeneous moving media.^{6,12,20}

Most studies on high amplitude wave propagation in turbulent air were motivated by a sonic boom problem. It is known that in homogeneous media a high amplitude acoustic pulse transforms to an N -shaped wave with two shocks. The width of the shocks is defined by the combined effects of nonlinearity, relaxation, and thermoviscous dissipation.^{17,21–23} However, differently shaped sonic booms are observed in a turbulent atmosphere—high amplitude U -waves, rounded waves, and waves with several peaks.^{24–26} It has been reported that both the subjective loudness and perceived annoyance of the sonic boom, when heard outdoors, are defined by the peak positive pressure and the rise times of shocks.^{27–29} Therefore, prediction of the acoustic field in a turbulent medium is important for estimating the annoyance of sonic booms in a turbulent atmosphere. However, experimental data obtained during supersonic flight tests are not sufficient to validate models because the amount of experimental data is limited to tens of supersonic flights per measurement

^{a)} Author to whom correspondence should be addressed. Electronic mail: misha@acs366.phys.msu.ru

^{b)} Also at: Center for Industrial and Medical Ultrasound, Applied Physics Laboratory, University of Washington, 1013 NE 40th Street, Seattle, WA 98105.

campaign,^{24,26} and because it is impossible to have a full description of atmospheric conditions. Therefore, model experiments have also been conducted to investigate the effects of turbulence on N -wave propagation.

The first laboratory scale experiments on the diffraction of shock waves on sound speed inhomogeneities were conducted by Davy and Blackstock.³⁰ Studying the propagation of spark-generated N -waves through a gas-filled soap bubble, they observed formation of U -waves in focusing zones and rounded waves outside them. More recently, another experiment dealing with scalar deterministic inhomogeneities was conducted by Ganjehi *et al.*³¹ The authors studied the diffraction of a sawtooth wave on a silicon phantom placed in a water tank, preserving good scaling of the experiment to the sonic boom problem. However, the results obtained cannot be directly applied to evaluate the effects of inhomogeneities on sonic booms, because the periodic nature of sawtooth waves results in better time coherence, stronger nonlinear dissipation, and weaker nonlinear refraction than for N -waves.^{6,12} Although these experiments provide insight about shock wave focusing in a medium with deterministic inhomogeneities, they do not address the problem of random focusing in a moving and randomly inhomogeneous medium, which requires statistical analysis.

Lipkens and Blackstock^{32,33} and Ollivier and Blanc-Benon³⁴ have shown that laboratory scale experiments using N -waves produced by electrical sparks and a downscaled turbulent medium offer an attractive alternative to field measurements since both the acoustic source and the turbulence can be well controlled. Distorted waveforms similar to those measured during supersonic flight tests^{24–26} were obtained in the scale experiments. Such experiments, which reproduce the properties of a randomly moving medium, were conducted both for plane and spherical wave propagation.^{32,33} However, the width of the turbulent layer in these experiments (0.05–0.5 m) was less than the distance of occurrence of the first caustic associated with the large turbulence scales.³⁵ Thus, only small-scale inhomogeneities in the random medium affected statistics of the measured acoustic waves. In addition, the short duration of the N -waves led to strong thermoviscous and relaxation-induced absorption, which was ten times stronger than that for a sonic boom propagating in a realistic atmosphere. The acoustic peak pressure (about 500 Pa at 15 cm from the source) was relatively low to produce strong nonlinear effects at larger distances.⁸

The effect of random caustics on acoustic field statistics was further investigated experimentally by Ollivier and Blanc-Benon.³⁴ Two types of random inhomogeneities were considered: Temperature (thermal) and velocity (kinematic) fluctuations. A plane free jet was used to generate velocity fluctuations, and a heated grid was used to generate temperature fluctuations. It was demonstrated that the temperature and velocity turbulence fluctuations resulted in different statistics of the acoustic wave parameters. The thermal turbulence setup was designed to investigate long-range propagation (0.6–4.4 m) for a fixed level of turbulence, while the kinematic turbulence setup allowed studying the effect of turbulence level on N -wave statistics only at shorter dis-

tances (up to 1 m). Thus, nonlinear propagation of shock pulses through kinematic turbulence over distances greater than the distance of occurrence of the first-order caustics associated with large-scale inhomogeneities has not been investigated in laboratory experiments.

In this paper we present new results obtained using an experimental setup that was designed to expand previous experimental studies of random focusing effect on statistics of a nonlinear acoustic field in a turbulent flow.^{32–34} Nonlinear focusing of spark-generated N -waves was studied at distances beyond the position of the first-order caustics related to the large-scale structures of turbulence. Turbulence was generated using a rectangular nozzle, which was larger than those used in the earlier experiments. Longer duration and higher amplitude N -waves were used to enhance the roles of nonlinear propagation and inhomogeneities relative to thermoviscous absorption and relaxation. Acoustic field parameters were analyzed as functions of the turbulence level and the propagation distance. Although the experimental setup was not designed to directly simulate the propagation of sonic booms, the scales and parameters of the experiment are comparable to those for sonic boom propagation in the atmosphere.

The paper is organized as follows: In Sec. II the experimental arrangement is described and parameters of the shock wave are defined. The results of accurate characterization of the turbulent velocity field are presented in Sec. III A. The effects of turbulence level and propagation distance through the turbulence on statistics of acoustic waves are analyzed in Secs. III C and III D, respectively. In Sec. III E the scaling of the laboratory experiment to a sonic boom geometry is discussed. Concluding remarks are given in Sec. IV.

II. EXPERIMENTAL METHOD

The experimental setup (Fig. 1) was built in two steps: First, a nozzle was designed to obtain a fully developed turbulent jet; second, an electric spark source was adjusted to generate high amplitude N -waves and installed at a side of the jet opposite to the microphones. The setup was installed in an anechoic chamber ($10 \times 8 \times 8 \text{ m}^3$).

The coordinate system was chosen as shown in Fig. 1. The center of the coordinates was located at the center of the nozzle exit; the x axis was the axis along the jet; the y axis was collinear with the direction from the spark source to microphone 2 (along the width of the nozzle); and the z axis was aligned vertically along the height of the nozzle. The source–microphone distance, measured along the y axis, is denoted as r . Acoustic measurements were performed at the distance $x = x_0 = 3.78 \text{ m}$ from the nozzle.

A. Experimental arrangement for generation and measurement of the turbulent velocity field

The turbulent field was generated as described by Gutmark and Wignanski,³⁶ using an intense airflow emanating from a large rectangular nozzle with a cross section of $160 \text{ mm} \times 1400 \text{ mm}$. Two baffles were fixed on the nozzle as shown in Fig. 1 in order to avoid spreading of the flow in the y direction, thus maintaining the level of turbulence.

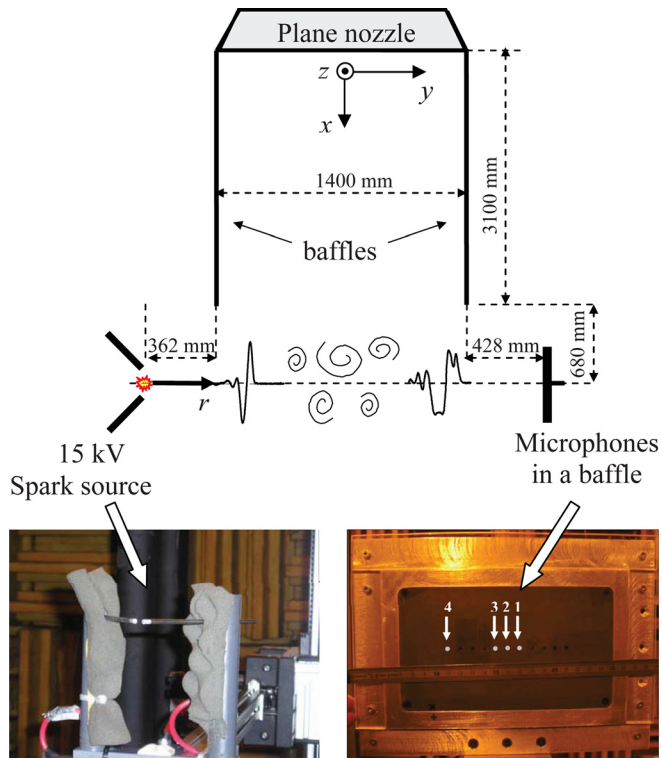


FIG. 1. (Color online) Sketch of the experimental setup (top view). Left photograph represents the spark source and the right photograph details the positions of the microphones (gray points) in the baffle.

Air temperature and humidity were measured during the experiments. Mean and fluctuating components of the velocity field were measured using DANTEC (Skovlunde, Denmark) X-wire probes (type 55P51) mounted on a computer controlled positioning system. Probes were calibrated before each measurement series in the potential core near the exit of the nozzle, where the flow was laminar.^{36,37} The mean flow velocity measured using a Pitot tube was used as a reference.

B. Experimental arrangement for generation and measurement of acoustic waves

Spherically divergent N -pulses were generated by a high voltage (15 kV) electric spark source as shown in Fig. 1. Detailed characterization of the source can be found in Refs. 8 and 38. Acoustic measurements were performed using four wideband 3 mm diameter condenser microphones (Brüel & Kjær, Mennecy, France, type 4138, -3 dB at 140 kHz) mounted in a baffle in order to postpone the diffracted waves (Fig. 1). Electric outputs from the microphones were amplified using a Brüel & Kjær Nexus amplifier with a bandwidth extended up to 200 kHz, and then digitally recorded at a 5 MHz sampling frequency using National Instrument data acquisition cards driven by LABVIEW. The voltage signals were then converted into pressure using the amplitude-frequency response of the measuring system.⁸ Acoustic measurements were triggered by the electromagnetic signal generated during the electric discharge of the spark source.

The repeatability of the source was checked by analyzing the statistics of N -wave parameters. The peak positive

pressure measured by a reference microphone positioned at 37 cm above the source was 290 ± 10 Pa; the half duration of the pulse was 13.16 ± 0.23 μ s; and the standard deviation of the arrival time was 1.7 μ s. Note that the measured rise time of the shock front at short distances from the source was significantly overestimated due to the limited bandwidth of the measuring system: The minimal measured rise time was about 2.5 μ s instead of 0.3 μ s as predicted theoretically and recently measured using an optical method.³⁸

To reduce waveform distortion induced by low frequency hydrodynamic perturbations, the microphones were placed about 40 cm to the side of the jet (Fig. 1). The first experiment was conducted to study the effect of the turbulence level on the acoustic field. In this experiment, the spark source was also placed outside the jet. The distance between the source and the microphones was fixed at $r = 2.19$ m so that the source and the microphones were not affected by the jet.

In order to study the effect of the propagation distance on the statistics of the acoustic field, the second experiment with the spark source located within the turbulent flow was performed. The turbulent flow influences N -wave generation by varying air temperature and humidity around the source, and by vibrating the mounting support. In order to evaluate this influence of varying air properties on N -wave statistics, the source was first switched off for several hours, then it was switched on and acoustic waveforms were recorded while the temperature and humidity changed around the source due to its self-heating over time. Acoustic measurements at $r = 2.19$ m showed negligible variations of pressure amplitudes (5%) and rise times (1%). Low frequency vibration of the mounting support, observed during experiments, resulted in slightly different propagation paths of the acoustic pulses: The maximum displacement was about 10 mm at a jet velocity of 20 m/s. Such a change in the propagation distance is estimated to have a negligible effect on the shock wave amplitude and the rise time:^{8,38} Thermoviscous absorption and nonlinear dissipation result in about a 0.5% change in pressure amplitude; spherical divergence causes additional peak pressure decrease of about 2%. Only the arrival time was significantly affected—a 10 mm change in the wave path causes about a 30 μ s time delay. Note that due to strong vibrations of the mounting support at high jet velocities such as 40 m/s at the nozzle, it was not possible to move the source deeper than 0.4 m inside the turbulent field. Therefore, measurements at short propagation distances have not been performed at high jet velocities.

C. Definition of acoustic wave parameters

Propagation in a turbulent medium leads to strong distortion of acoustic waveform, so that it is not always obvious how to define peak positive pressure and rise time. For example, if waveforms with several peaks or several shocks are considered, definitions for peak positive pressure and rise time should be refined.³⁴ Acoustic wave parameters are usually defined as follows: Peak positive pressure p_+ is the maximum pressure in the waveform, which is usually the maximum pressure of the first positive peak; rise time t_{sh} is the time needed for the pressure to increase from $0.05 p_+$ to

$0.95 p_+$ at the front shock; arrival time t_{art} of the pulse is calculated at 10% level of the maximum pulse pressure.^{8,32,34} These definitions are used in the literature for waveforms measured both in still and turbulent media. However, this definition for rise time cannot be effectively applied to complex waveforms with multiple peaks or several jumps on the waveform, which are often measured in turbulent flows.³⁴

In this paper, classical definitions for p_+ and t_{art} are used and a new definition for the rise time is proposed, as illustrated in Fig. 2. Shown in Fig. 2(a) is an N -wave measured in homogeneous air at a distance $r = 210$ mm from the spark source. The waveform is not symmetric, some oscillations are present, and its back slope does not show a linear decrease as would be present for an ideal N -wave. In relaxing motionless air, the front shock of the acoustic wave is very well approximated by the stationary solution to the Burgers equation.^{8,21} Note that the time needed for pressure to increase from $0.05 p_+$ to $0.95 p_+$ equals the width of the peak of the pressure derivative at the level D/e , where D is the maximum derivative value and e is Euler's number ($e \approx 2.7$). Therefore, it is proposed here to define the rise time of the shock t_{sh} based on the time derivative of the pressure profile: The shock rise time is the width of the highest peak of the pressure derivative at the level D/e . Note that the

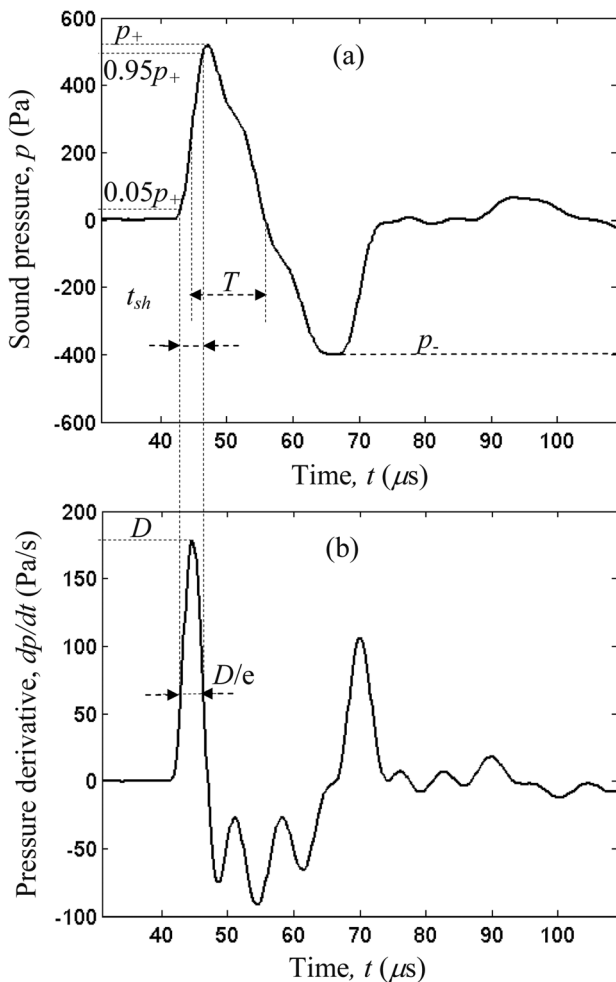


FIG. 2. (a) Typical waveform measured in motionless air at a distance 210 mm from the spark source and (b) its time derivative.

pressure waveform was smoothed to minimize the effects of high frequency noise in calculating the derivative. As shown in Fig. 2(b) for waves propagating in motionless air, classical and new definitions are equivalent. For waves propagating in turbulent media these definitions of the rise time t_{sh} give different results. An advantage of the new definition is that the rise time is obtained according to the steepness of the shock; therefore, two close shocks connected with a smooth junction will never be considered as one long shock. Moreover, shocks situated in the tail part of the wave will be detected automatically. These properties are very important for estimating the perceived loudness of sonic booms, which is sensitive to short, steep, and high amplitude shocks regardless of shock positions within the waveform.^{28,29}

The arrival time shift Δt_{art} of the wave for each series of measurements was calculated taking into account the temperature dependence of sound speed: $c_0(T) = (\gamma RT/m)^{1/2}$, where γ is the specific heat ratio, R is the absolute gas constant, and m is the gas molecular weight. The shift of the arrival time is then $\Delta t_{\text{art}} = t_{\text{art}} - r/c_0(T)$, so that in a motionless medium $\Delta t_{\text{art}}(0) = 0 \mu\text{s}$.

III. RESULTS AND DISCUSSION

A. Characterization of the turbulent velocity field

The turbulent field was characterized by the mean and fluctuating components of airflow velocity. Velocity profiles $[U(x,y,z), V(x,y,z), W(x,y,z)]$ were measured for different jet velocities at the nozzle $U_{\text{jet}} = \langle U(0,0,0) \rangle$, where angular brackets denote a time average. In the experiment the jet nozzle velocity varied from 0 to 40 m/s. At the distance $x_0 = 3.78$ m from the nozzle where acoustic measurements were acquired, the axial component of the mean flow velocity $\langle U(x_0, y, z) \rangle$ was as high as 20 m/s. Fluctuating velocities $u = U - \langle U \rangle$, $v = V - \langle V \rangle$, and $w = W - \langle W \rangle$ were extracted from the measured velocity profiles, and the turbulence levels were found as $u_{\text{rms}} = \sqrt{\langle u^2 \rangle}$, $v_{\text{rms}} = \sqrt{\langle v^2 \rangle}$, and $w_{\text{rms}} = \sqrt{\langle w^2 \rangle}$.

The flow velocity patterns mapped at the distance $x = x_0$ are shown in Fig. 3 for the jet nozzle velocity $U_{\text{jet}} = 40$ m/s. The axial component of the mean flow velocity $\langle U(x_0, y, z) \rangle$ is normalized to the jet nozzle velocity U_{jet} [Fig. 3(a)]. The pattern shows a rapid decrease of $\langle U(x_0, y, z) \rangle$ in the z direction while moving away from the jet axis and a moderate increase along the y direction, which is followed by a fast drop around $y = \pm 700$ mm. The maximum of mean flow velocity is achieved near the edge of the jet at $y = \pm 600$ mm. Lateral y and z components of the mean flow velocity $\langle V \rangle$ and $\langle W \rangle$ were negligible and are not shown here. The x and y components of the turbulence intensity, $u_{\text{rms}}/U_{\text{mean}}$ and $v_{\text{rms}}/U_{\text{mean}}$, respectively, are shown in Figs. 3(b) and 3(c). Here, $U_{\text{mean}} = \langle U(x_0, 0, 0) \rangle$. The distributions are nonuniform; however, it is possible to identify a region along the acoustic propagation path where the components of turbulence intensity are almost constant. Regions where the variation of turbulence intensity does not exceed 10% are denoted in Figs. 3(b) and 3(c) with contour lines. Inside these regions the turbulence intensities are, on average, equal to $u_{\text{rms}}/U_{\text{mean}} = 0.26$ and $v_{\text{rms}}/U_{\text{mean}} = 0.22$.

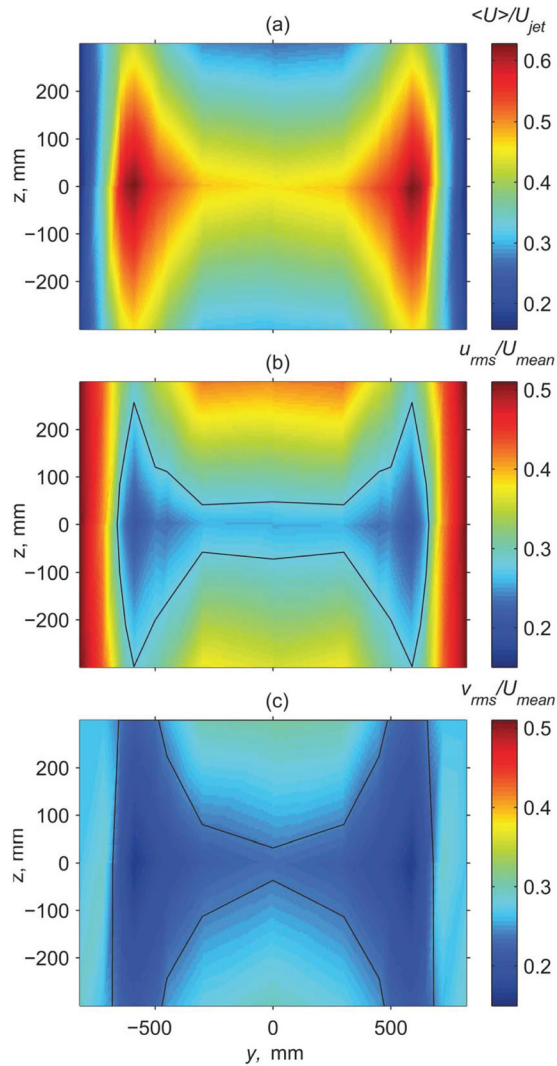


FIG. 3. (Color online) (a) Distribution of normalized mean flow velocity $\langle U \rangle / U_{\text{jet}}$; (b), (c) the intensities of turbulent fluctuations $u_{\text{rms}} / U_{\text{mean}}$, and $v_{\text{rms}} / U_{\text{mean}}$. Measurements were performed at a distance $x_0 = 3.78$ m from the nozzle with $U_{\text{jet}} = 40$ m/s. Contour lines $u_{\text{rms}} / U_{\text{mean}} = 0.28$ and $v_{\text{rms}} / U_{\text{mean}} = 0.24$ denote the area where turbulence is statistically homogeneous and isotropic.

According to Gutmark and Wynanski,³⁶ at these intensities the turbulence can be assumed to be fully developed, i.e., statistically homogeneous and isotropic. The self-preservation region was $z \in [-50, 50]$ mm, $y \in [-650, 650]$ mm at $U_{\text{jet}} = 40$ m/s and remained almost unchanged at other values of the jet nozzle velocity. The results of measurements summarized in Table I demonstrate that both the mean and root-mean-square (rms) values of fluctuating velocity measured on axis at $x_0 = 3.78$ m were directly proportional to the jet nozzle velocity: $U_{\text{mean}} \approx 0.43U_{\text{jet}}$, $u_{\text{rms}} \approx 0.1U_{\text{jet}}$, and $v_{\text{rms}} \approx 0.083U_{\text{jet}}$. Taking into account these relations and recalling that the distortion of the acoustic field is caused mainly by turbulence fluctuations in the direction of wave propagation path,^{6,12} only the on-axis value of v_{rms} will be reported further in the text, and it will be referred to as “turbulence level.”

Note that estimated shifts of wave paths caused by the presence of mean flow are smaller than the width of the self-preservation region. Therefore, most of the acoustic wave propagation paths lay inside this region. This conclusion is

TABLE I. Mean flow velocity U_{mean} measured on axis at $x_0 = 3.78$ m, rms values of the fluctuating velocity u_{rms} and v_{rms} , and distance to the first caustic r_{caust} [see Eq. (4)] as a function of the jet nozzle velocity U_{jet} .

U_{jet} (m/s)	15.0	20.0	25.0	30.0	35.0	40.0
U_{mean} (m/s)	6.4	8.6	11.0	13.3	15.5	17.6
u_{rms} (m/s)	1.5	1.9	2.4	3.1	3.5	3.9
v_{rms} (m/s)	1.1	1.6	1.9	2.5	3.0	3.4
r_{caust} (mm)	2890	2327	2077	1790	1604	1503

very important for numerical modeling and comparison between simulated and experimental results as it allows the application of isotropic turbulence models.^{12,39,40}

Shown in Fig. 4 is the one-dimensional spatial spectrum of the turbulence [$E_{11}^{\text{exp}}(K_1)$, jagged curve] measured at the distance $(x_0, 0, 0)$. The spectrum was obtained as follows: (1) Time series of the velocity fluctuations (2–3 min) were used to calculate the single-point frequency-domain spectrum $E(f)$ of the turbulence fluctuations; (2) the Taylor hypothesis of a turbulent structure transfer by mean flow⁴¹ was applied $E_{11}^{\text{exp}}(K_1) = E(f)U_{\text{mean}} / (2\pi)$. Here $K_1 = 2\pi f / U_{\text{mean}}$ is the absolute value of the x component of the turbulence wave vector \mathbf{K} ($K = \sqrt{K_1^2 + K_2^2 + K_3^2}$). The experimental spectrum is compared to the Kolmogorov’s “ $-5/3$ ” power law (solid line) and the one-dimensional modified von Kármán spectrum $E_{11}^{\text{Karm}}(K_1)$ (smooth curve), obtained by integrating the three-dimensional (3D) spectrum:³⁷

$$E_{11}^{\text{Karm}}(K_1) = \int_{K_1}^{\infty} E_{3D}^{\text{Karm}}(K) (1 - (K_1/K)^2) / 2K dK,$$

$$E_{3D}^{\text{Karm}}(K) \cong 1.45 u_{\text{rms}}^2 L_0^{-2/3} K^4 (K^2 + L_0^{-2})^{-17/6} \cdot \exp(-(K/K_m)^2). \quad (1)$$

Here $K_m = 5.92/l_0$, while L_0 and l_0 are the outer and inner scales of turbulence fluctuations. It is seen in Fig. 4 that the spectrum of generated turbulence has an inertial interval (Kolmogorov’s hypothesis) limited by the outer and inner scales, and is very well fitted by the modified von Kármán spectrum $E_{11}^{\text{Karm}}(K_1)$ with $l_0 = 1.7$ mm and $L_0 = 200$ mm. A good agreement between the experimental and analytical spectra confirms statistical isotropy and homogeneity of the turbulent flow.

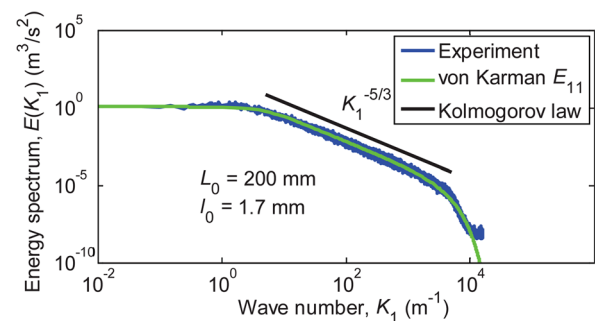


FIG. 4. (Color online) Comparison of the measured turbulence spectrum (jagged curve) with the modified von Kármán spectrum (smooth curve) and the Kolmogorov “ $-5/3$ ” power law (solid line). Measurements were done at $x_0 = 3.78$ m on the jet axis with $v_{\text{rms}} = 3.4$ m/s.

Comparison of inner and outer scales deduced from turbulence spectra measured at different points in the yz plane at $x_0 = 3.78$ m are presented in Fig. 5. The spectra of axial u (left column) and transverse v (right column) components of velocity fluctuations are shown for $v_{\text{rms}} = 3.4$ m/s at the locations $(x_0, 100 \text{ mm}, 0)$, $(x_0, 500 \text{ mm}, 0)$, and $(x_0, 720 \text{ mm}, 0)$. All experimental results agree well with the analytic von Kármán formulation $E_{11}^{\text{Kármán}}(K_1)$ with corresponding outer and inner scales shown in each subplot. At the first two points [(a)–(d)] located inside the self-preservation region (Fig. 3) the inner and outer turbulent scales vary slightly within a 10% interval: $l_0 \in [1.5 \text{ mm}, 1.7 \text{ mm}]$ and $L_0 \in [200 \text{ mm}, 220 \text{ mm}]$. Outside the turbulence self-preservation region [(e)–(f)], estimated scales were significantly different: $L_0 = 150 \text{ mm}$ and $l_0 = 1.0 \text{ mm}$. In fact, the model Eq. (1) is not valid here, as the turbulence becomes unstationary and anisotropic. Similar results were obtained at other turbulence levels v_{rms} .

In experimental studies on turbulence, another scale is often used—the integral scale, which can be deduced from measured data without making any assumptions about the shape of the turbulence spectrum.³⁷ If the assumptions are made and the turbulence spectrum is described by Eq. (1), then the longitudinal integral scale L_f of the turbulence is related to the value of its energy spectrum at low wave numbers as

$$L_f = \pi \frac{E_{11}(K_1 = 0)}{u_{\text{rms}}^2} = 0.747L_0 \quad (2)$$

and therefore is directly proportional to the outer scale L_0 . In the current experiment the longitudinal integral scale $L_f \in [150 \text{ mm}, 164 \text{ mm}]$.

A direct method to obtain the integral scale without any assumptions on the spectrum shape is to integrate the measured correlation function $R_{ij}^{(k)}$. Here $R_{ij}^{(k)}$ denotes the normalized correlation of i th and j th components of the velocity field with the location of the probe along the k axis. For example, $R_{12}^{(2)}$ is the correlation function of u and v velocity profiles with the displacement along the y axis:

$R_{12}^{(2)} = \langle u(\mathbf{r})v(\mathbf{r} + d\mathbf{y}) \rangle / \sqrt{\langle u(\mathbf{r})^2 \rangle \langle v(\mathbf{r} + d\mathbf{y})^2 \rangle}$. According to the Kármán–Howarth relation for isotropic turbulence, all autocorrelation functions with displacement in the direction of the correlating flow component are equal and are usually defined as the longitudinal correlation function f . All autocorrelation functions with displacement in the direction transverse to the correlating flow component are also equal and are usually defined as the transverse correlation function g . The longitudinal integral scale L_f is related to the transverse integral scale as $L_f = 2L_g$.^{36,37} Using this relation and the definition of the transverse integral scale L_g , the longitudinal integral scale can be obtained as³⁷

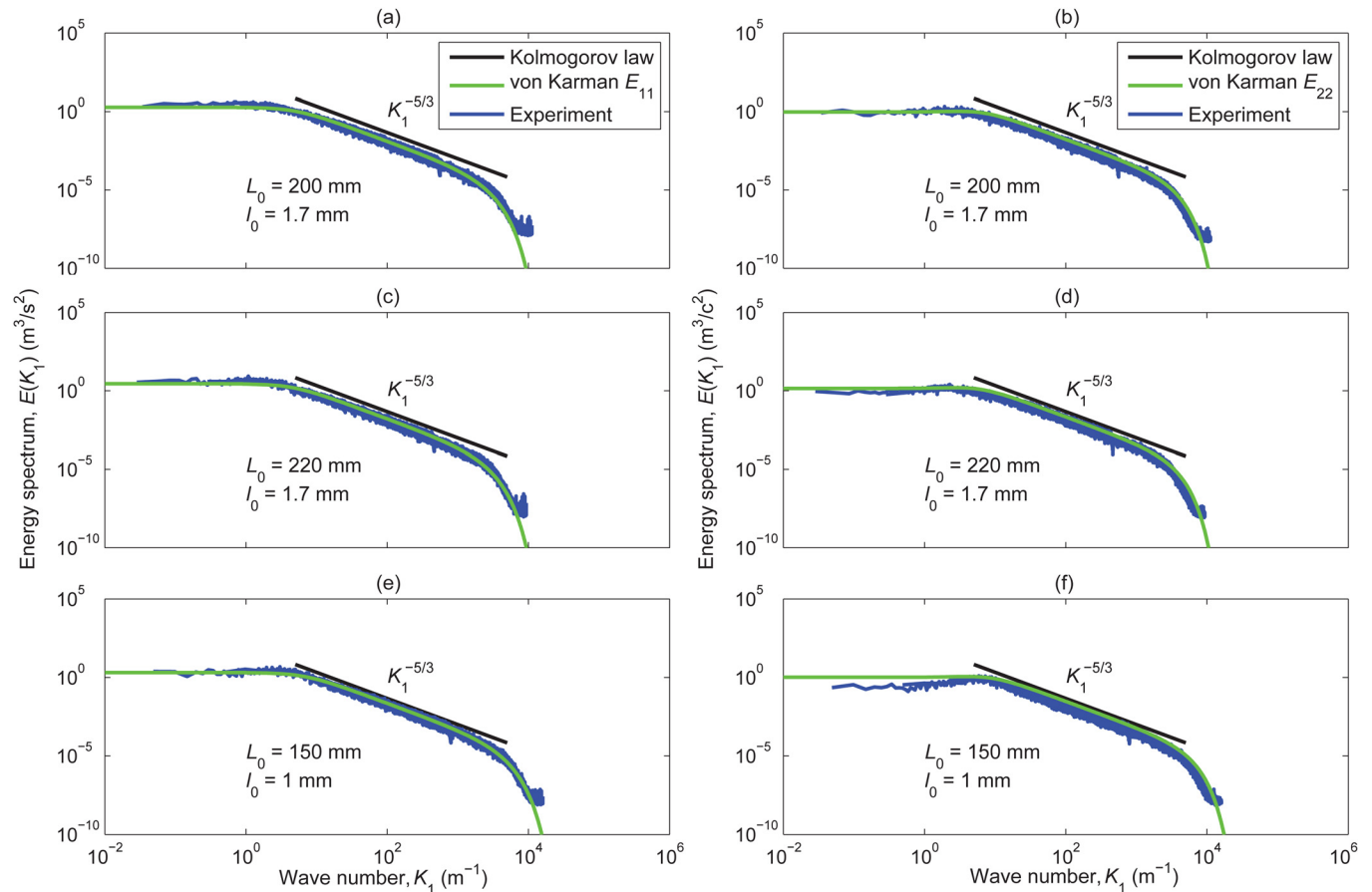


FIG. 5. (Color online) Spatial spectra of the longitudinal u (left) and transverse v (right) components of medium velocity fluctuations (jagged curves) measured at different points of the yz plane: (a), (b) at $(x_0, 100, 0)$ mm, (c), (d) at $(x_0, 500, 0)$ mm, and (e), (f) at $(x_0, 720, 0)$ mm. Smooth curve—modified von Kármán spectrum; solid line—Kolmogorov’s $-5/3$ power law ($v_{\text{rms}} = 3.4$ m/s).

$$L_f = 2L_g = 2 \int_0^\infty g \, dy = 2 \int_0^\infty R_{11}^{(2)} \, dy = 2 \int_0^\infty R_{11}^{(3)} \, dz. \quad (3)$$

Shown in Fig. 6 are the longitudinal correlation functions $R_{11}^{(2)}$ measured at $(x_0, 0, 0)$ mm (circles) and at $(x_0, -350, 0)$ mm (diamonds). During the measurements, both probes were positioned inside the homogeneous part of the turbulent field. Measured correlation functions have slightly different shapes mainly due to changes in flow characteristics and environmental conditions during the experiment, which typically lasted about 1 h. The longitudinal correlation function $R_{11}^{(3)}$ (asterisks) was calculated from measurements with the first probe fixed at $(x_0, -350 \text{ mm}, 0)$ and the second probe moving along the z axis leaving the area of fully developed turbulence at $z \approx 150$ mm (see Fig. 3). This agrees well with the distance where the difference between $R_{11}^{(3)}$ and $R_{11}^{(2)}$ becomes notable. Faster loss of correlation is observed in the inhomogeneous turbulence. Finally, integration of correlation functions measured inside the area of fully developed turbulence gave the longitudinal integral scale as $L_f = 2L_g \in [160, 182]$ mm.

Note that both direct and indirect methods for estimation of the longitudinal integral length scale L_f give similar results. This agreement shows the accuracy of the acquired measurements and also ensures the validity of the modified von Kármán formulation for the numerical modeling of turbulent fields in the context of sound wave propagation.⁶

B. Acoustic waveform measurements

Acoustic measurements were performed at the distance $x_0 = 3.78$ m from the nozzle with the source–microphone distance $r = 2.19$ m (Fig. 1). Typical acoustic waveforms became distorted after propagation through the turbulent flow and are shown in Fig. 7. Experimental waveforms similar to sonic boom waveforms were measured:^{24–26,42} (a) Classical N -wave; (e) high amplitude U -waves with narrow shock fronts; (c) rounded waves; and (d) waves with several shock fronts or (b) several peaks. Various pulse amplitudes, rise times, and arrival times were observed. It was found that

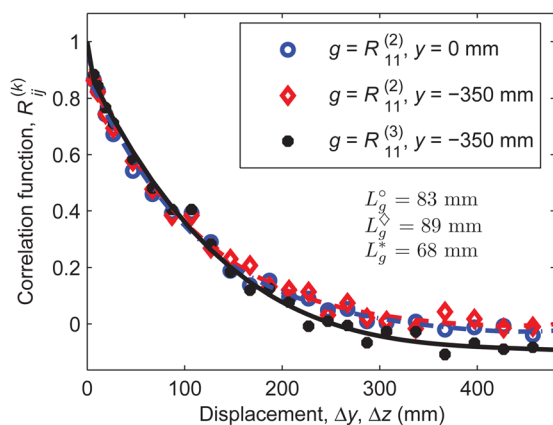


FIG. 6. (Color online) Autocorrelation functions of the u component of the turbulent velocity field ($v_{\text{rms}} = 3.4$ m/s) at $(x_0, 0, 0)$ mm and $(x_0, -350, 0)$ mm. Circles and diamonds indicate horizontal displacement and asterisks indicate vertical displacement, both along the y axis. Dashed-dotted, dashed, and solid curves are the corresponding fits.

low amplitude waves arrived earlier than high amplitude waves. All measured waveforms had oscillations in the tail part after the negative peak. Several waveforms with the maximum pressure and the minimum rise time located in the tail part of the wave were observed (f). The maximum pressure, therefore, did not always correspond to the front shock.

C. Effect of turbulence level on statistical and peak characteristics of the acoustic N -wave

In order to compute waveform statistics as a function of turbulence level, 2000 pulses were emitted and recorded for each jet velocity using four microphones located at the source–microphone distance $r = 2.19$ m. The variations of mean wave characteristics as functions of the level of turbulence fluctuations v_{rms} are presented in Fig. 8. Individual measurements are shown as dots, mean values are shown with solid lines, and standard deviations with vertical bars. Random focusing of acoustic waves in turbulent air resulted in a more than threefold increase of the peak positive pressure p_+ compared to the peak pressure in motionless air [Fig. 8(a)]. On the other hand, very low peak pressures (more than a tenfold reduction) were observed in regions of wave defocusing. As the regions of high pressure level were small and the regions of low pressure level were large, the mean peak positive pressure $\langle p_+ \rangle$ (angular brackets denote the ensemble average) in a turbulent medium was smaller than that for the motionless air.¹² With an increase of the turbulence intensity the mean peak positive pressure decreased. At the highest turbulence level, $v_{\text{rms}} = 3.4$ m/s, $\langle p_+ \rangle = 22.0$ Pa as compared to $\langle p_+ \rangle = 30.9$ Pa for the motionless air.

In a homogeneous medium, the rise time of a nonlinear acoustic shock front is directly proportional to its amplitude.^{8,38} In a turbulent medium this relation is only valid locally in focusing zones, where pressures are high enough to induce nonlinear effects, and is not valid in low pressure defocusing regions. Therefore, due to destructive interference the mean rise time of shocks in a turbulent medium is likely to increase faster than it would be estimated from the mean peak pressure. Indeed, Fig. 8(b) shows an almost two-fold increase of the rise time from $4.0 \mu\text{s}$ in homogeneous air to about $7.9 \mu\text{s}$ in turbulent air with $v_{\text{rms}} = 3.4$ m/s, while the change in peak pressure is only 40%.

Figure 8(c) shows that on average in the turbulent medium the wave arrives faster than in motionless air: the mean arrival time shift $\langle \Delta t_{\text{art}} \rangle = \langle t_{\text{art}} - r/c_0 \rangle$ decreases with the increase of the turbulence level v_{rms} . For example, propagation time from the spark source to the microphone in the turbulent medium ($v_{\text{rms}} = 3.4$ m/s) is, on average, $26 \mu\text{s}$ shorter than in the motionless medium. This result is consistent with the Fermat least action principle, which when applied to acoustics states that in a motionless medium wave propagates so as to minimize travel time.⁴³

Shown in Fig. 9 are statistical distributions of (a) the peak positive pressure and (b) the rise time at different turbulence levels: $v_{\text{rms}} = 0, 1.1, 1.6, 1.9, 2.5, 3.0,$ and 3.4 m/s. Each distribution comes from the analysis of 8000 waveforms (2000 sparks, 4 microphones). The distributions in motionless air ($v_{\text{rms}} = 0$ m/s) also have finite widths due to

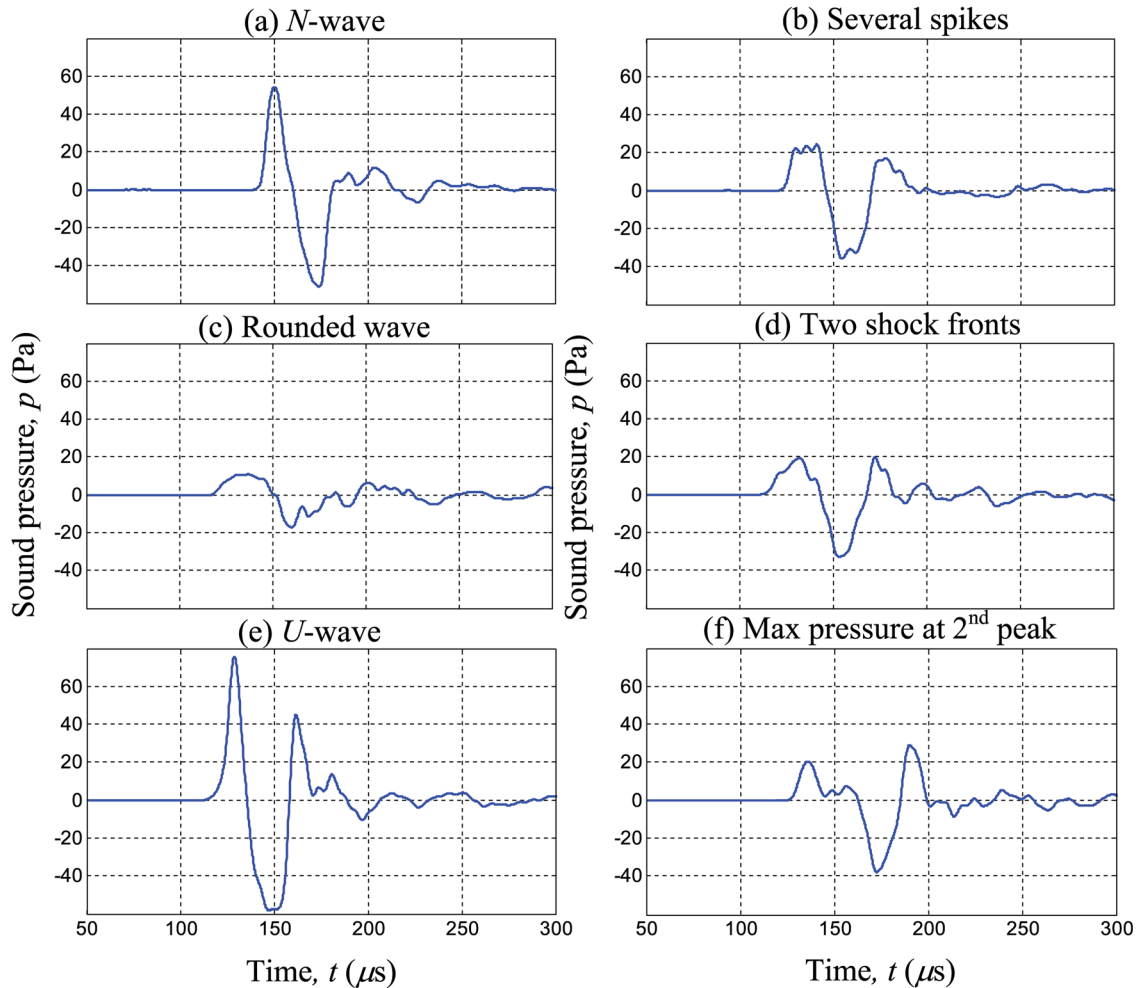


FIG. 7. (Color online) Typical waveforms distorted by turbulence and measured at 2.19 m from the spark source. $v_{\text{rms}} = 2.5$ m/s.

slightly different source–microphone distances and fluctuations in shock wave pressure generated by the spark source. In addition, differences in the frequency responses of microphones also introduce some distortion of the probability distributions. In turbulent air, the peak positive pressure distributions broaden significantly: A long tail forms at high pressure values, similar to the results of Ref. 34. With the increase of v_{rms} , the distribution maximum shifts to lower amplitudes as has been shown for the mean value in Fig. 8(a). However, notwithstanding the decrease of the mean peak positive pressure, occasional high amplitude peaks were observed, with the amplitude more than three times higher than in homogeneous air at the same distance $r = 2.19$ m. For example, the observation probability of a twofold increase in pressure amplitude achieves its maximum at $v_{\text{rms}} = 1.6$ m/s and is equal to 2%.

The standard deviation of peak positive pressure, σ_p , exhibits a fast increase from 2.7 Pa in motionless air to 11 Pa in turbulent air with $v_{\text{rms}} = 1.6$ m/s (Fig. 9). At higher turbulence levels the standard deviation saturates and slowly achieves its maximum of 12 Pa at $v_{\text{rms}} = 2.5$ m/s. Saturation of the standard deviation is associated with the limited band of the turbulence spectrum (Fig. 4). Each turbulence scale L in the spectrum results in the formation of random caustics mostly at distances longer than the characteristic distance to

the first caustic. This latter distance can be estimated for the multi-scale turbulence represented as a set of single-scale turbulent fields with Gaussian energy spectra. In the geometrical acoustics approximation one can obtain the distance to the first caustics as¹⁰

$$r_{\text{caust}} \approx 0.286L(c_0/v_{\text{rms}})^{2/3} + r_{\text{turb}}, \quad (4)$$

where $r_{\text{turb}} \approx 200$ mm is the distance between the spark source and the turbulence boundary and $c_0 = 337$ m/s is the sound speed. Small-scale turbulent structures of size $L = l_0$ lead to focusing before the microphones: $r_{\text{caust}} < 400$ mm for all experimental levels of the turbulence fluctuations. Large turbulence scales of size $L = L_0$ induce focusing before microphones ($r_{\text{caust}} < 2.19$ m) only if the turbulence level v_{rms} is sufficiently high (see Table I, $v_{\text{rms}} = 1.9$ m/s). Thus, the initial increase in turbulence level resulted in more foci associated with large turbulence scales formed at the microphone position. As the presence of such scales results in higher focusing gains, the standard deviation of the peak positive pressure increases. According to Table I, at $v_{\text{rms}} = 1.9$ m/s, most of the energy-containing turbulence scales $L \in [l_0, L_0]$ yielded random foci before the microphones. There was little energy at larger turbulence scales, and caustics associated with them did not give sufficiently

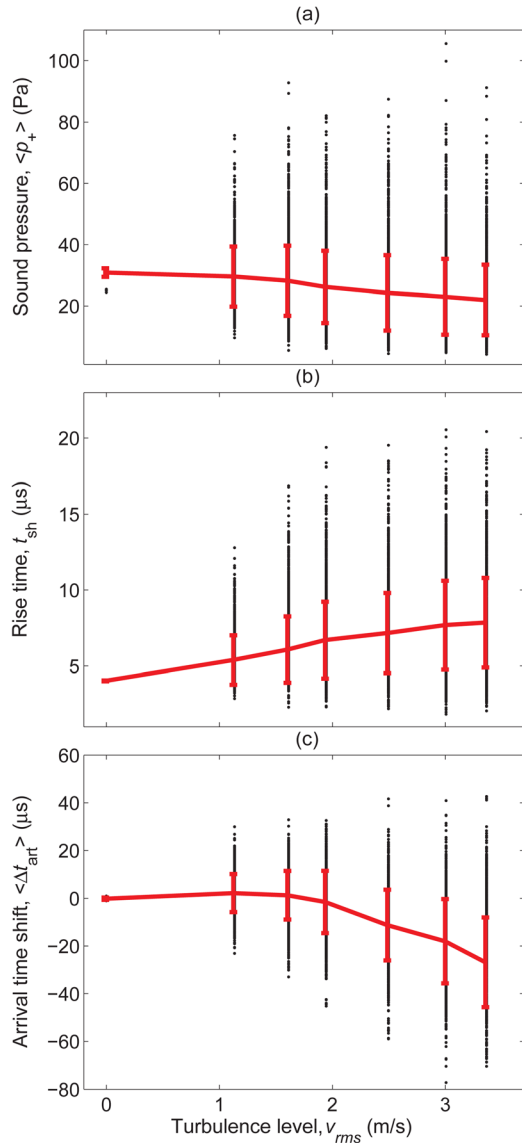


FIG. 8. (Color online) (a) Mean peak positive pressure, (b) mean rise time of the shock front, and (c) mean arrival time of the wave, as functions of the turbulence level v_{rms} measured at $r = 2.19$ m. Vertical segments are the standard deviations. Individual measurements are shown with points.

high gains to increase the standard deviation of the peak positive pressure. Therefore the value of σ_p saturated with further increases in turbulence level.

Large-scale inhomogeneities have further importance. Caustics induced by large-scale turbulent structures produced the strongest changes in the mean peak positive pressure and the mean arrival time. At turbulence levels higher than $v_{rms} = 1.6$ m/s, $\langle p_+ \rangle$ and $\langle \Delta t_{art} \rangle$ decreased quickly [Figs. 8(a) and 8(c)], because random foci associated with scales $L \sim L_0$ start to form at the microphone positions. In contrast, the rate of increase of the mean rise time of shocks was not sensitive to changes in turbulence level, and therefore large-scale structures had little impact [Fig. 8(b)]. The mean rise time increased with the turbulence level mainly due to the cumulative effects of small-scale turbulent structures, which is in accordance with results obtained from numerical modeling.¹²

It has been previously reported that a probability distribution of the harmonic wave intensity measured in thermal

turbulence is well described by the generalized gamma distribution.⁴⁴ This distribution was shown to be applicable to a wide range of experimental conditions. We have tested the relevance of this model to describe statistical distributions of the parameters of shock pulses measured after propagation through kinematic turbulence. According to Stacy,⁴⁵ the generalized gamma distribution that approximates the probability density for peak positive pressure at different turbulence levels can be cast as

$$W(p_+, v_{rms}) = \frac{a}{c\Gamma(b)} (p_+/c)^{ab-1} e^{-(p_+/c)^a}, \quad (5)$$

where $\Gamma(b)$ is the gamma function and the coefficients a , b , and c are functions of the turbulence level v_{rms} , which varies from 1.1 to 3.4 m/s. The coefficients a and b are shape parameters and c is a scale parameter. Using the least-square method in the standard fitting function of MATLAB, it was possible to estimate all three parameters. The best fit of generalized gamma distributions to the experimental statistics shown in Fig. 9 is achieved for $c = 0.98$, and for a and b as represented in Fig. 10. Variations of the shape coefficients can be fitted as functions of turbulence level by third-order polynomials with 95% confidence (dotted curves). Thus, statistical properties of the acoustic wave amplitude are described by two parameters in Eq. (5), which are elementary functions of the turbulence level. As turbulence level increases, b decreases to produce a shift of the probability distribution maximum towards low pressure values. Moreover, a decreases to produce a slower exponential decrease at high turbulence levels and, therefore, an increase in the

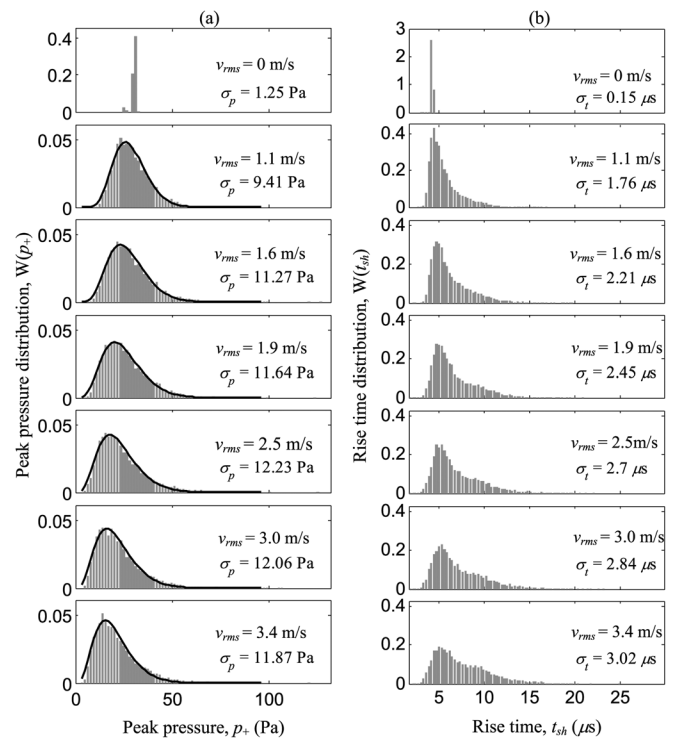


FIG. 9. (a) Probability distributions of peak positive pressure and (b) rise time for various turbulence levels v_{rms} at $r = 2.19$ m. Black curves represent fits of the peak pressure distributions using Eq. (5). The bin widths are 2 Pa and 0.5 μs , respectively. σ_p and σ_t are standard deviations.

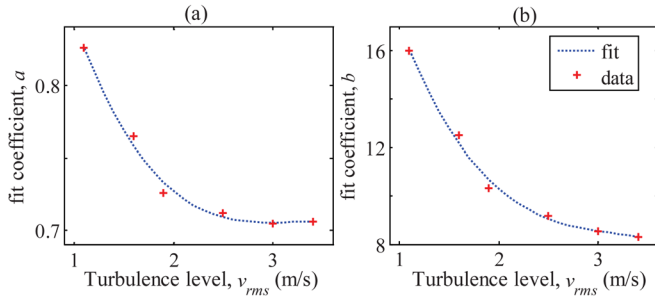


FIG. 10. (Color online) Dependence of a and b coefficients in the generalized gamma distribution [Eq. (5)] on the turbulence level v_{rms} .

occurrence of high pressure amplitudes. In the limit of $v_{rms} \rightarrow \infty$, the distribution shape should first transform to a decreasing exponent and then to a delta function ($a \rightarrow \infty$) as acoustic waves would be completely scattered by inhomogeneities. Therefore, generalized gamma distributions can be used to fit the probability density functions of the peak positive pressure measured in turbulent velocity fields in conditions of both weak and strong scattering. Finally, the probability distribution of peak positive pressure possesses a similarity property with respect to the level of turbulence fluctuations. The probability distribution at any turbulence level can be obtained using Eq. (5) and coefficients found from Fig. 10. One important property of the generalized gamma distribution [Eq. (5)] is that its moments can be easily found analytically.⁴⁵

$$M_n(v_{rms}) = \frac{c^n \Gamma(b + n/a)}{n! \Gamma(b)}, \quad (6)$$

where n is the order of the moment M_n . This permits determination of the mean (M_1) and the standard deviation ($\sigma = \sqrt{M_2 - M_1^2}$) of peak positive pressure based on known parameters of the generalized gamma distribution a and b (c is constant as shown earlier). Alternately, the inverse problem can be solved to determine the parameters of the distribution by solving a set of nonlinear equations (6) for an experimentally measured mean and standard deviation.

The probability density distributions of peak positive pressure obtained using Eq. (5) at different turbulence levels are shown in Fig. 9 with black curves. An overall good agreement with experimental data is achieved. The linear model given by Eq. (5) fits the experimental data very well at low pressure amplitudes $p_+ < 40$ Pa. The discrepancies become more pronounced at higher amplitudes, $p_+ > 40$ Pa, presumably because of nonlinear effects, which are stronger for higher pressures.

The rise time probability distributions [Fig. 9(b)] show both short and long wave fronts. Short rise times are primarily due to enhanced nonlinear focusing of the acoustic wave and related steepening of the front,^{6,17} while long rise times are caused by a loss of coherence between pulses that arrive from different directions. As destructive interference caused by the loss of coherence dominates nonlinear steepening, most of the rise times measured in the turbulent medium are longer than those measured in still air, and the distribution

maximum moves to high values. However, the shortest rise times in the turbulent medium $t_{sh} \approx 2-3 \mu s$ were shorter than the rise time of the pulse measured in homogeneous air $t_{sh} \approx 4 \mu s$. In contrast to pressure distributions, the shape of rise time distributions is strongly asymmetric and at low turbulence levels it can be approximated by a right triangle. The minimum measured rise time, $t_{sh} \approx 2-3 \mu s$, was the same for all turbulence levels v_{rms} despite theoretical predictions and optical measurements that suggest shorter time values.^{8,38} Actually, the minimal measured rise time was determined by the limited frequency response of the measuring system.⁸ Thus, shorter fronts were smoothed by the microphones to $2-3 \mu s$, which resulted in a high occurrence rate of these values at low turbulence levels $v_{rms} < 2.5$ m/s [Fig. 9(b)]. At higher turbulence levels, due to destructive interference, fewer waveforms with rise times of the order of $2-3 \mu s$ were formed. The probability of observing this value decreased and the shape of the distribution changed from a triangular shape to a bell-like shape with a long tail at high rise times.

D. Effect of propagation distance in a turbulent medium on the N -wave statistics

Measurement data obtained with the source moving inside the jet along the y axis were analyzed to compute the statistics of wave parameters as functions of propagation distance and turbulence level. Shown in Fig. 11 are (a) the mean peak positive pressure and (b) the mean rise time resulting from analysis of 2000 waveforms measured by

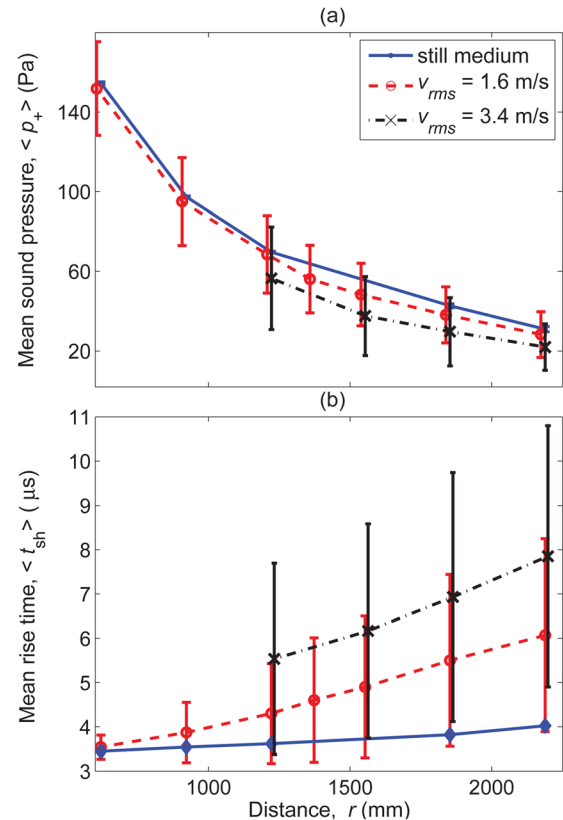


FIG. 11. (Color online) (a) Dependence of the mean peak positive pressure, and (b) the mean rise time on the distance of propagation in turbulent air. Vertical bars show the standard deviation, σ_p and σ_r .

microphone 2 (Fig. 1) for each distance and turbulence level. The solid curve corresponds to motionless air, the dashed curve to $v_{\text{rms}} = 1.6$ m/s, and the dashed-dotted curve to $v_{\text{rms}} = 3.4$ m/s. Corresponding standard deviations are indicated with vertical bars.

Here, turbulence affected N -wave parameters in a way similar to what was shown in Fig. 8: It decreased the mean peak positive pressure and increased the mean rise time compared to measurements in motionless medium. However, up to the propagation distance $r = 1200$ mm, the mean peak positive pressures in turbulent air (dashed curve, $v_{\text{rms}} = 1.6$ m/s) and in homogeneous air (solid curve) are almost equivalent. The effect of turbulence on the peak pressure becomes apparent only at $r \approx 1500$ – 1700 mm, where turbulence scales on the order of L_0 ($L \in [130$ – $150]$ mm) start to induce focusing before the microphones [Eq. (4)]. At the level of $v_{\text{rms}} = 3.4$ m/s, changes in the peak pressure become more pronounced. Stronger differences between motionless and turbulent cases are observed as more turbulence scales are involved in the focusing at the microphones. At longer distances, the difference between turbulent and still air cases becomes smaller due to faster dissipation of waves in motionless air, as they contain more energy at higher frequencies. Indeed, as can be seen in Fig. 11(b), the mean rise time of the acoustic wave is always longer in turbulent air than in still air. High frequency content of the wave in still air is rapidly suppressed by excessive absorption, thereby equalizing mean peak positive pressures in turbulent and homogeneous air at long propagation distances. Note also that in contrast to mean peak positive pressure, the rate of increase of mean rise time [Fig. 11(b)] does not depend on propagation distance: The dependence is almost linear. The cumulative effect of small turbulence scales of the turbulence on mean rise time is therefore suggested to be dominant.

It can be seen that the standard deviation of the peak positive pressure [bars in Fig. 11(a)] decreases as the spark source moves further away from the microphone because wave energy dissipates and nonlinear enhancement of focusing becomes less intensive. Moreover, focusing of waves at long distance becomes a rare phenomenon due to the loss of coherence.¹² However, the relative value of standard deviation $\sigma_p/\langle p_+ \rangle$ increases. For example, at a distance $r = 1800$ mm from the source for $v_{\text{rms}} = 3.4$ m/s, the standard deviation becomes approximately equal to the mean peak positive pressure $\sigma_p/\langle p_+ \rangle \simeq 1$, suggesting probability of waveforms with peak positive pressure close to zero.

E. Characteristic scales: Sonic boom and laboratory experiment

Characteristic spatial and time scales of the sonic boom problem^{24,25,42} are compared to scales of the laboratory experiment in Table II. The width of the turbulent boundary layer (1–2 km) and turbulence integral scale (100–200 m)^{46,47} in the sonic boom problem are well scaled to the geometry of the laboratory experiment with a scaling ratio of 1:1000. Mean values of wind velocity during sonic boom experiments have ranged up to 15 m/s,²⁴ and rms

TABLE II. Comparison of spatial and time scales of the sonic boom problem with the laboratory scale experiment.

	Atmosphere	Laboratory scale experiment
Turb. layer width, d	1–2 km	0.3–1.8 m
Integral length scale, L_f	100–200 m	16–18 cm
rms velocity, v_{rms}	0–2.5 m/s	0–3.4 m/s
Mean velocity, U_{mean}	0–15 m/s	0–20 m/s
Pressure amplitude, p_+	10–100 Pa	10–100 Pa
Pulse duration, T	0.1–0.2 s	30–80 μ s
Rise time, t_{sh}	0.5–10 ms	(0.8)–20 μ s
Normalized nonlinear distance $x_{\text{nonl}}/c_0 T^a$	200	400

^a x_{nonl} is the distance at which the amplitude of the plane N -wave decreases by a factor of $\sqrt{2}$.

values of fluctuating velocity in atmospheric turbulence measurements have ranged up to 2.5 m/s.^{46,47} These ranges are well scaled by the present laboratory experiment. However, stratification of the atmosphere was not reproduced in our laboratory experiment.

A typical sonic boom profile formed by a 30 m long conventional aircraft (small military fighter or business jet) and measured at the ground level has a pressure amplitude lower than 100 Pa, a duration of 0.15–0.20 s, and a rise time varying between 0.5 and 10 ms.^{24–26} The initial pressure amplitude of the N -wave in the laboratory scale experiment was chosen to be much higher than the typical amplitude of the sonic boom in order to compensate for spherical spreading and to attain the same order of nonlinear effects in terms of the characteristic nonlinear distance.^{8,21} Even though the initial amplitude of the pulse in our experiment was almost twice higher than that in the studies of Lipkens and Blackstock³³ (1300 compared to 750 Pa at 0.1 m from the source), it was not sufficient to fully reproduce the nonlinear effects at a similar level as in the sonic boom problem. However, at distances of 1–2 m, which scale the sonic boom propagation distance in the atmospheric boundary layer (1–2 km), pulse amplitudes varied between 10 and 100 Pa, which is typical for sonic booms.

One more point is that the laboratory scale experiment was also performed in air, thus neither the thermoviscous dissipation coefficients, nor the properties of oxygen and nitrogen relaxation were scaled. The plane wave attenuation coefficient at typical sonic boom frequencies (about 10 Hz) is of the order of 10^{-6} m^{-1} , and at spark-generated N -wave frequencies (about 50 kHz) is of the order of 10^{-2} m^{-1} .¹⁷ Moreover, shock rise time in the model experiment is mostly governed by thermoviscous dissipation, while in the case of sonic boom the dominant mechanism is molecular relaxation.^{8,23} This leads to an overestimation of rise time in the laboratory scale experiment, which is much less important than the overestimation induced by the limited frequency response of the microphones.⁸ However, according to the results of Ref. 8, the minimum value of the rise time in the laboratory scale experiment is estimated to be about 0.8 μ s, which corresponds to 100 Pa shock pressure amplitude.

IV. CONCLUSIONS

A series of laboratory scale experiments was reported in which the spherical propagation of high amplitude (about 1000 Pa) and short duration (about 25 μ s) acoustic N -pulses through a fully characterized turbulent layer was investigated. It was shown that the energy spectrum of the generated turbulence is well described by the modified von Kármán spectrum for statistically homogeneous and isotropic turbulence. The influence of both turbulence level and propagation distance on the distortion of N -waves was investigated. It was shown that the effect of scaled turbulence on the acoustic N -wave propagation was similar to that of atmospheric turbulence on sonic boom waveforms. Distortion of the initial N -wave led to the formation of classical U -shape waves, rounded waves, waves with several shock fronts, and others. The influence of turbulence resulted in a strong variation of shock rise time and pressure amplitude. On average, in the turbulent flow, acoustic pressure amplitude decreased and rise time increased both with higher levels of turbulence and with longer source–microphone distances. In addition, the acoustic arrival times were shorter in turbulent air than in the still air. However, in approximately 20% of the cases, waveforms with amplitudes higher than those measured in motionless air were observed, including waveforms with a threefold increase in amplitude.

Probability density distributions of acoustic pressure amplitude were shown to have a similarity property with respect to turbulence level. Both in conditions of weak and strong scattering, experimental data were found to be well described by generalized gamma distributions, which smoothly vary from a log-normal to an exponential distribution when the turbulence level was increased. Since the generalized gamma distribution appears to represent the experimental data for a large range of turbulence levels, it will be of interest to model the statistical effects of turbulence on N -wave propagation using appropriately designed random filters as proposed by Locey and Sparrow.⁴⁸

In turbulent air, large-scale fluctuations dominated the decrease of mean pressure amplitude and arrival time, while small-scale fluctuations were responsible for the loss of coherence and the associated increase in the mean rise time. Mean pressure amplitude behavior was well correlated with the first caustic formation distance given by large-scale perturbations of the order of the outer turbulence scale.

A result of this well documented experiment is also a complete database that can be used to test models of nonlinear sound propagation in kinematic turbulence. However, the limited frequency response of the measurement systems distorted experimental waveforms, thus complicating the estimation of the shock rise times. Therefore, when comparing experimental results with the results of numerical modeling, it is necessary to take into account the influence of microphone frequency response.³⁸

ACKNOWLEDGMENTS

This work was partially supported by the Russian Foundation for Basic Research and Centre National de la Recherche Scientifique (Projet International de Cooperation Scientifique

RFBR 10-02-91062/CNRS 5063). The authors express their thanks to Pascal Souchotte, Emmanuel Jondeau, and Jean-Michel Perrin for assistance in designing the experimental setup and in performing some of the measurements. The authors also thank G. A. Maksimov for fruitful discussions of the experimental results and W. Kreider for helpful comments on the manuscript.

- ¹L. Evers and H. W. Haak, "The characteristics of infrasound, its propagation and some early history," in *Infrasound Monitoring for Atmosphere Studies*, edited by A. Le Pichon, E. Blanc, and A. Hauchecorne (Springer, Dordrecht, 2010), pp. 3–27.
- ²A. A. Piacsek, "Atmospheric turbulence conditions leading to focused and folded sonic boom wavefronts," *J. Acoust. Soc. Am.* **111**, 520–529 (2002).
- ³H. E. Bass, R. Raspet, J. P. Chambers, and M. Kelly, "Modification of sonic boom waveforms during propagation from the source to the ground," *J. Acoust. Soc. Am.* **111**, 481–486 (2002).
- ⁴S. N. Kulichkov, "Long-range propagation and scattering of low-frequency sound pulses in the middle atmosphere," *Meteorol. Atmos. Phys.* **85**, 47–60 (2004).
- ⁵I. P. Chunchuzov, S. N. Kulichkov, A. Otrezov, and V. G. Perepelkin, "Acoustic pulse propagation through a fluctuating stably stratified atmospheric boundary layer," *J. Acoust. Soc. Am.* **117**, 1868–1879 (2005).
- ⁶M. V. Aver'yanov, V. A. Khokhlova, O. A. Sapozhnikov, P. Blanc-Benon, and R. O. Cleveland, "Parabolic equation for nonlinear acoustic wave propagation in inhomogeneous moving media," *Acoust. Phys.* **52**, 623–632 (2006).
- ⁷R. Marchiano, F. Coulouvrat, and J.-L. Thomas, "Nonlinear focusing of acoustic shock waves at a caustic cusp," *J. Acoust. Soc. Am.* **117**, 566–577 (2005).
- ⁸P. V. Yuldashev, M. V. Aver'yanov, V. A. Khokhlova, S. Ollivier, and P. Blanc-Benon, "Nonlinear spherically divergent shock waves propagating in a relaxing medium," *Acoust. Phys.* **54**, 32–41 (2006).
- ⁹H. E. Bass, J. Ezell, and R. Raspet, "Effect of vibrational relaxation on rise times of shock waves in the atmosphere," *J. Acoust. Soc. Am.* **74**, 1514–1517 (1983).
- ¹⁰P. Blanc-Benon, D. Juvé, and G. Comte-Bellot, "Occurrence of caustics for high-frequency acoustic waves propagating through turbulent fields," *Theor. Comput. Fluid Dyn.* **2**, 271–278 (1991).
- ¹¹V. A. Kulkarny and B. S. White, "Focusing of waves in turbulent inhomogeneous media," *Phys. Fluids* **25**, 1770–1784 (1982).
- ¹²M. Aver'yanov, P. Blanc-Benon, R. O. Cleveland, and V. Khokhlova, "Nonlinear and diffraction effects in propagation of n -waves in randomly inhomogeneous moving media," *J. Acoust. Soc. Am.* **129**, 1760–1772 (2011).
- ¹³M. V. Aver'yanov, V. A. Khokhlova, R. O. Cleveland, and P. Blanc-Benon, "Nonlinear and diffraction effects in propagation of shock N -wave in randomly inhomogeneous moving media," in *Proceedings of the XIX Session RAO*, Nizhny-Novgorod, Russia (September 24–28, 2007), Vol. 1, pp. 105–108.
- ¹⁴R. Marchiano, F. Coulouvrat, and R. Grenon, "Numerical simulation of shock wave focusing at fold caustics, with application to sonic boom," *J. Acoust. Soc. Am.* **114**, 1758–1771 (2003).
- ¹⁵R. Blumrich, F. Coulouvrat, and D. Heimann, "Meteorologically induced variability of sonic-boom characteristics of supersonic aircraft in cruising flight," *J. Acoust. Soc. Am.* **118**, 707–722 (2005).
- ¹⁶V. E. Ostashev, *Acoustics in Moving Inhomogeneous Media* (E&F Spon, London, 1997), pp. 27–89.
- ¹⁷A. D. Pierce, *Acoustics: An Introduction to Its Physical Principles and Applications* (McGraw-Hill, New York, 1981), pp. 566–619.
- ¹⁸A. D. Pierce, "Statistical theory of atmospheric turbulence effects on sonic-boom rise times," *J. Acoust. Soc. Am.* **49**, 906–924 (1971).
- ¹⁹D. I. Blokhintsev, *Acoustics of a Nonhomogeneous Moving Medium* (Science, Moscow, 1946) [English translation, NASA Tech. Memo. **1399**, 1–74 (1956)].
- ²⁰B. Lipkens, "Model experiment to study sonic boom propagation through turbulence. Part III: Validation of sonic boom propagation models," *J. Acoust. Soc. Am.* **111**, 509–519 (2002).
- ²¹O. V. Rudenko and S. I. Soluyan, *Theoretical Foundations of Nonlinear Acoustics* (Consultants Bureau, New York, 1977), pp. 42–65.
- ²²R. O. Cleveland, J. P. Chambers, H. E. Bass, R. Raspet, D. T. Blackstock, and M. F. Hamilton, "Comparison of computer codes for the propagation

- of sonic boom waveforms through isothermal atmospheres," *J. Acoust. Soc. Am.* **100**, 3017–3027 (1996).
- ²³A. D. Pierce, "Molecular relaxation effects on sonic boom waveforms: A tutorial survey," *J. Acoust. Soc. Am.* **92**, 2329–2339 (1992).
- ²⁴R. A. Lee and J. M. Downing, "Sonic booms produced by US Air Force and US Navy aircraft: Measured data," Technical Report, Armstrong Lab Brooks AFB, TX, Accession number ADA244804 (1991), <http://www.dtic.mil/docs/citations/ADA244804> (Last viewed 8/29/2011).
- ²⁵K. R. Elmer and M. C. Joshi, "Variability of measured sonic boom signatures," in *High-Speed Research: Sonic Boom* (Langely Research Center, Hampton, VA, 1994), Vol. 1, pp. 191–218.
- ²⁶D. A. Hilton, H. H. Hubbard, V. Huckel, and D. J. Maglieri, "Ground measurements of sonic-boom pressures for the altitude range of 10,000 to 75,000 feet," Technical Report No. NASA-TR-R-198, NASA (1964).
- ²⁷J. D. Leatherwood, B. M. Sullivan, K. P. Shepherd, D. A. McCurdy, and S. A. Brown, "Summary of recent NASA studies of human response to sonic booms," *J. Acoust. Soc. Am.* **111**, 586–598 (2002).
- ²⁸A. Niedzwiecki and H. S. Ribner, "Subjective loudness of sonic-boom: N-wave and minimized (low-boom) signatures," *J. Acoust. Soc. Am.* **64**, 1622–1626 (1978).
- ²⁹D. J. Maglieri and H. W. Carlson, "The shock wave noise problem of supersonic aircraft in steady flight," Technical Report No. NASA-MEMO-3-4-59L, NASA (1959).
- ³⁰B. A. Davy and D. T. Blackstock, "Measurements of the refraction and diffraction of a short N-wave by a gas-filled soap bubble," *J. Acoust. Soc. Am.* **49**, 732–737 (1971).
- ³¹L. Ganjehi, R. Marchiano, F. Coulouvrat, and J.-L. Thomas, "Evidence of wave front folding of sonic booms by a laboratory-scale deterministic experiment of shock waves in a heterogeneous medium," *J. Acoust. Soc. Am.* **124**, 57–71 (2008).
- ³²B. Lipkens and D. T. Blackstock, "Model experiment to study sonic boom propagation through turbulence. Part I: Model experiment and general results," *J. Acoust. Soc. Am.* **103**, 148–158 (1998).
- ³³B. Lipkens and D. T. Blackstock, "Model experiment to study sonic boom propagation through turbulence. Part II: Effect of turbulence intensity and propagation distance through turbulence," *J. Acoust. Soc. Am.* **104**, 1301–1309 (1998).
- ³⁴S. Ollivier and P. Blanc-Benon, "Model experiment to study acoustic N-wave propagation through turbulence," in *10th AIAA/CEAS Aeroacoustics Conference*, Manchester, UK (2004), paper No. AIAA2004-2921.
- ³⁵P. Blanc-Benon, D. Juvé, V. E. Ostashev, and R. Wandelt, "On the appearance of caustics for plane sound-wave propagation in moving random media," *Waves Random Media* **5**, 183–199 (1995).
- ³⁶E. Gutmark and I. Wignanski, "The planar turbulent jet," *J. Fluid Mech.* **73**, 465–495 (1976).
- ³⁷G. Comte-Bellot and C. Bailly, *Turbulence* (CNRS, Lyon, France, 2003), pp. 133–183.
- ³⁸P. V. Yuldashev, M. V. Averiyarov, V. A. Khokhlova, O. A. Sapozhnikov, S. Ollivier, and P. Blanc-Benon, "Nonlinear propagation of spark-generated N-waves in air: Modeling and measurements using acoustical and optical methods," *J. Acoust. Soc. Am.* **128**, 3321–3333 (2011).
- ³⁹M. Karweit, P. Blanc-Benon, D. Juvé, and G. Comte-Bellot, "Simulation of the propagation of an acoustic wave through a turbulent velocity field: A study of phase variance," *J. Acoust. Soc. Am.* **89**, 52–62 (1991).
- ⁴⁰P. Blanc-Benon, B. Lipkens, L. Dallois, M. F. Hamilton, and D. T. Blackstock, "Propagation of finite amplitude sound through turbulence: Modeling with geometrical acoustics and the parabolic approximation," *J. Acoust. Soc. Am.* **111**, 487–498 (2002).
- ⁴¹A. S. Monin and A. M. Yaglom, *Statistical Fluid Mechanics: The Mechanics of Turbulence* (MIT Press, Cambridge, MA, 1975), Vol. 2, pp. 7–30.
- ⁴²E. A. Haering, L. J. Ehernberger, and S. A. Whitmore, "Preliminary airborne measurements for the SR-71 sonic boom propagation experiment," Technical Report No. NASA TM-104307, NASA (1995).
- ⁴³B. Iooss, P. Blanc-Benon, and C. Lhuillier, "Statistical moments of travel times at second order in isotropic and anisotropic random media," *Waves Random Media* **10**, 381–394 (2000).
- ⁴⁴P. Blanc-Benon and D. Juvé, "Intensity fluctuations of spherical acoustic waves propagating through thermal turbulence," *Waves Random Media* **3**, 71–83 (1993).
- ⁴⁵E. W. Stacy, "A generalization of the gamma distribution," *Ann. Math. Stat.* **33**, 1187–1192 (1962).
- ⁴⁶R. Frehlich, Y. Meillier, M. L. Jensen, B. Balsley, and R. Sharman, "Measurements of boundary layer profiles in an urban environment," *J. Appl. Meteorol.* **45**, 821–837 (2006).
- ⁴⁷I. Smalikho, F. Köpp, and R. Rham, "Measurement of atmospheric turbulence by 2- μ m Doppler Lidar," *J. Atmos. Oceanic Technol.* **22**, 1733–1747 (2005).
- ⁴⁸L. L. Locey and V. W. Sparrow, "Modeling atmospheric turbulence as a filter for sonic boom propagation," *Noise Control Eng. J.* **55**, 495–503 (2007).